




ORIGINAL ARTICLE

OPEN

Adeno-associated virus serotype 2 capsid variants for improved liver-directed gene therapy

Nadja Meumann^{1,2}  | Marti Cabanes-Creus³ | Moritz Ertelt^{4,5} |
 Renina Gale Navarro³ | Julie Lucifora⁶  | Qinggong Yuan^{7,8} | Karin Nien-Huber⁹ |
 Ahmed Abdelrahman⁹ | Xuan-Khang Vu¹ | Liang Zhang^{2,10} |
 Ann-Christin Franke¹ | Christian Schmithals¹¹ | Albrecht Piiper¹¹ |
 Annabelle Vogt¹² | Maria Gonzalez-Carmona¹² | Jochen T. Frueh¹³ |
 Evelyn Ullrich¹³ | Philip Meuleman¹⁴ | Steven R. Talbot¹⁵ |
 Margarete Odenthal^{2,10}  | Michael Ott^{7,8} | Erhard Seifried⁹ | Clara T. Schoeder⁴ |
 Joachim Schwäble⁹ | Leszek Lisowski^{3,16} | Hildegard Büning^{1,2} 

¹Institute of Experimental Hematology, Hannover Medical School, Hannover, Germany

²Center for Molecular Medicine Cologne, University of Cologne, Cologne, Germany

³Translational Vectorology Research Unit, Children's Medical Research Institute, The University of Sydney, Sydney, New South Wales, Australia

⁴Institute for Drug Discovery, University Leipzig Medical School, Leipzig, Germany

⁵Center for Scalable Data Analytics and Artificial Intelligence ScaDS.AI, Dresden/Leipzig, Germany

⁶Cancer Research Center of Lyon, Institut National de la Santé et la Recherche Médicale, Lyon, France

⁷Department of Gastroenterology, Hepatology, and Endocrinology, Hannover Medical School, Hannover, Germany

⁸Twincore Centre for Experimental and Clinical Infection Research, Hannover, Germany

⁹Institute for Transfusion Medicine and Immunohematology, Goethe University Hospital Medical School, German Red Cross Blood Donor Service, Frankfurt, Germany

¹⁰Institute of Pathology, University Hospital Cologne, Cologne, Germany

¹¹Department of Internal Medicine I, University Hospital Frankfurt, Frankfurt, Germany

¹²Department of Internal Medicine I, University Hospital Bonn, Bonn, Germany

¹³Experimental Immunology, Children's University Hospital, Goethe University Frankfurt, Frankfurt am Main, Germany

¹⁴Laboratory of Liver Infectious Diseases, Faculty of Medicine and Health Sciences, Ghent University, Ghent, Belgium

¹⁵Institute for Laboratory Animal Science, Hannover Medical School, Hannover, Germany

¹⁶Military Institute of Medicine, Laboratory of Molecular Oncology and Innovative Therapies, Warsaw, Poland

Abbreviations: AAV, adeno-associated virus; Ab, antibody; BALB/c, bagg albino; BC, barcode; cDNA, complementary DNA; ELISA, enzyme-linked immunosorbent assay; FIX, blood clotting factor 9; Fluc, firefly luciferase; GOI, gene of interest; HB, hemophilia B; HCC, hepatocellular carcinoma; FRG, Fah^{-/-}Rag2^{-/-}Il2rg^{-/-} mouse; hFRG, humanized FRG; HH, human hepatocyte; HSPG, heparan sulfate proteoglycan; i.v., intravenously; MD, molecular dynamic; MH, murine hepatocyte; NaCl, sodium chloride; NGS, next-generation sequencing; PHH, primary human hepatocyte; PMH, primary murine hepatocyte; ss, single-stranded; vg, viral genome containing particle;

Joachim Schwäble, Leszek Lisowski, and Hildegard Büning contributed equally.

Supplemental Digital Content is available for this article. Direct URL citations appear in the printed text and are provided in the HTML and PDF versions of this article on the journal's website, www.hepjournal.com.

This is an open-access article distributed under the terms of the Creative Commons Attribution-Non Commercial License 4.0 (CCBY-NC), where it is permissible to download, share, remix, transform, and buildup the work provided it is properly cited. The work cannot be used commercially without permission from the journal. Copyright © 2023 The Author(s). Published by Wolters Kluwer Health, Inc. on behalf of American Association for the Study of Liver Diseases.

Correspondence

Hildegard Büning, Institute of Experimental Hematology, Hannover Medical School, Carl-Neuberg-Str. 1, 30625 Hannover, Germany.
Email: buening.hildegard@mh-hannover.de

Funding information

BMBF and MWK Lower Saxony-funded Professorinnenprogramm Niedersachsen, Grant/Award Number: N/A; Deutsche Krebshilfe, Grant/Award Number: 109256; DFG-funded cluster of excellence REBIRTH, Grant/Award Number: N/A; Günter Landbeck Excellence Award 2015

Abstract

Background and Aims: Current liver-directed gene therapies look for adeno-associated virus (AAV) vectors with improved efficacy. With this background, capsid engineering is explored. Whereas shuffled capsid library screenings have resulted in potent liver targeting variants with one first vector in human clinical trials, modifying natural serotypes by peptide insertion has so far been less successful. Here, we now report on two capsid variants, MLIV.K and MLIV.A, both derived from a high-throughput *in vivo* AAV peptide display selection screen in mice.

Approach and Results: The variants transduce primary murine and human hepatocytes at comparable efficiencies, a valuable feature in clinical development, and show significantly improved liver transduction efficacy, thereby allowing a dose reduction, and outperform parental AAV2 and AAV8 in targeting human hepatocytes in humanized mice. The natural heparan sulfate proteoglycan binding ability is markedly reduced, a feature that correlates with improved hepatocyte transduction. A further property that might contribute to the improved transduction efficacy is the lower capsid melting temperature. Peptide insertion also caused a moderate change in sensitivity to human sera containing anti-AAV2 neutralizing antibodies, revealing the impact of epitopes located at the basis of the AAV capsid protrusions.

Conclusions: In conclusion, MLIV.K and MLIV.A are AAV peptide display variants selected in immunocompetent mice with improved hepatocyte tropism and transduction efficiency. Because these features are maintained across species, MLIV variants provide remarkable potential for translation of therapeutic approaches from mice to men.

INTRODUCTION

Adeno-associated virus (AAV) vectors are the most frequently used delivery system for *in vivo* gene therapy.^[1] Their remarkable clinical potential is testified among others by market approvals of AAV-based advanced therapy medicinal products^[2] and the great success in liver-directed hemophilia gene therapy trials.^[3] AAV vectors are composed of a protein capsid that protects a single-stranded (ss) DNA genome and determines the vector tropism.^[4]

When applied *in vivo*, host factors like serum proteins or neutralizing antibodies interact with the AAV capsid, impacting transduction efficiency and biodistribution.^[5] Likewise, interaction with cell surface molecules determines whether or not AAV vectors are internalized and shuttled toward a functional transduction pathway, eventually leading to transgene expression. Components of the extracellular matrix, such as heparan sulfate proteoglycan (HSPG), mediate the initial cell contact, thereby supporting AAV

binding to coreceptors^[6] that induce clathrin-dependent endocytosis of the particles. Furthermore, AAV receptor (AAVR) and G protein-coupled receptor (GPR) 108 escort AAV's intracellular processing,^[7,8] eventually leading to uncoating, i.e., the vector genome release from the viral capsid,^[9,10] and formation of stable episomes.^[11]

The capsid has become the target of engineering,^[4] aiming for improved transduction efficiencies and avoidance of vector loss in off-target tissues. Further desired features are translatability of vector efficacy and tropism from small to large animal models and, most importantly, to the human context. So far, efforts have mainly focused on shuffled DNA capsid libraries that were screened *in vivo* in various mouse models.^[12–14] To the best of our knowledge, shuffled capsid variant LK03^[12] is the first to be currently tested in phase 1/2 (NCT03003533, Spark 200).^[15]

Here, we report on liver-targeting capsid variants, MLIV.K and MLIV.A, derived from an *in vivo* AAV2 peptide display library selection in immunocompetent

mice, which transduce murine and human hepatocytes significantly better than the parental serotype. Significantly fewer particles were required for efficient liver transduction compared with the state-of-the-art reference AAV8. This improved efficiency was accompanied by detargeting from off-target tissues, such as spleen. Both variants showed impaired binding to HSPG, the tropism-defining attachment receptor of AAV2, and differed in a moderate but relevant range regarding sensitivity to AAV2 neutralizing-antibody-containing human sera.

MATERIAL AND METHODS

Human and animal ethics

All experiments involving human- and animal-derived samples received and followed ethical authorization and regulations. Human samples were involved according to the guidelines of the 1975 Declaration of Helsinki. Animals received human care according to the criteria outlined in the NIH Guide for the Care and Use of Laboratory Animals, respectively (see further details to ethical approvals in extended methods).

AAV library selection

Hepa129-transplanted C3H mice^[16] and transforming growth factor α /c-myc mice,^[17] $n = 1-2$, were intravenously (i.v.) injected with 1×10^{11} viral genome containing particles (vg)/animal (AAV2 peptide display library^[18]). After 24 h, the viral genomes of capsid variants were PCR amplified from DNA isolated from hepatocellular carcinoma (HCC) tissue from the nuclear fraction, and after the third selection round, capsid variants were recovered from the nuclear fraction of liver tissue as well as from other off-target tissues as described^[19] (see further details in extended methods).

Primary hepatocyte transduction

Primary human hepatocytes (PHH) were freshly prepared from surgical human liver biopsies by a standard two-step collagenase perfusion and serial differential centrifugation and cultured as described.^[20] Primary murine hepatocytes (PMH) were obtained from bagg albino (BALB/c) mice after liver perfusion and low-speed centrifugation and were cultured as described.^[21] After 2 days, cells were transduced with 1×10^4 vg/cell (genomic particles of infection [GOI]). Medium was changed 24 h later, followed by cell harvest 72 h post-transduction.

In vivo imaging

BALB/c mice, $n = 6$, were i.v. injected with 4×10^{11} vg/animal (scAAV.SFFV.Fluc with AAV2, AAV8, MLIV.K, and MLIV.A capsid). On Days 7, 15, and 28, luciferin D was i.v. injected followed by *in vivo* imaging system (IVIS) analysis of firefly luciferase (Fluc) activity. On Day 28, mice were euthanized and fresh frozen tissue conservation was performed.

Therapeutic treatment of hemophilia B (HB) mice

Blood clotting factor 9 (FIX) knockout mice (B6.129P2-F9tm1DWS/J), $n = 7-10$, were i.v. injected with 5×10^{10} vg/animal (scAAV.LP1.hFIX with AAV2, AAV8, MLIV.K, and MLIV.A capsid). Healthy C57Bl/6 (Bl6) ($n = 10$) and mock-treated HB ($n = 9$) were used as control mice. After serum collection on Day 7, Day 14, and Day 56, factor (F)IX activity assays and human (h)FIX enzyme-linked immunosorbent assay (ELISA) were performed as described.^[22,23] FIX activity of serum samples was determined through activated partial thromboplastin time with an hFIX standard curve. hFIX serum level were analyzed using an ELISA in which a monoclonal anti-hFIX antibody (Ab) (Sigma-Aldrich) was used as capture Ab. Peroxidase-conjugated polyclonal goat anti-hFIX Ab (Affinity Biologicals) was used as the detecting Ab.

Humanized mouse transduction

Naive Fah^{-/-}/Rag2^{-/-}/Il2rg^{-/-} (FRG) mice were housed and engrafted with an intrasplenic injection of human hepatocytes (HH) as described (comparison 1: 2.4–2.8 mg human serum albumin (hAlb)/ml \triangleq ~30% replacement index [RI = engraftment]; comparison 2: 6.4–8.0 mg hAlb/ml \triangleq RI of ~60% to ~80%).^[24] For IHC analysis of xenograft liver transduction, $n = 1$ animal received 5×10^{10} vg/vector (i.v.; ssAAV.LSP.eGFP.BC vectors with AAV2, AAV8, MLIV.K, and MLIV.A capsid). After 1 week, engrafted liver tissues were conserved and IHC stained.^[24] For a direct comparison of the AAV capsids, $n = 1$ (comparison 1; ssAAV.LSP.eGFP.BC vectors; eight unique barcodes [BC]/capsid; AAV2, AAV8, MLIV.K, and MLIV.A capsid) or $n = 2$ (comparison 2; ssAAV.LSP.eGFP.BC vect; eight unique BCs/capsid; AAV8, AAV3.B, LK03, NP59, SYD12, MLIV.K, and MLIV.A capsid) animal(s) received the corresponding vector pools (i.v., 1×10^{10} vg/vector) followed by liver perfusion after 1 week (comparison 1) or 2 weeks (comparison 2). Human and murine hepatocyte populations were isolated by fluorescence-activated cell sorting (FACS).^[24] Further, RNA and DNA isolation, BC amplification, and next-generation sequencing (NGS) as well as

distribution analysis of BC were performed^[24] (see further details in the extended methods).

Heparin affinity and competition assay

For heparin affinity chromatography, scAAV.CMV.eGFP vectors with AAV2, MLIV.K, or MLIV.A capsid were loaded on HiTrap Heparin HP columns (Cytiva). Particles were eluted in phosphate-buffered saline/MgCl₂/KCl supplemented with increasing concentrations of sodium chloride (NaCl).^[25] For competition assay, Pop10 cells (hepatocyte cell line) were seeded in 48-well plates. scAAV.SFFV.Fluc vectors (GOI 1000) were incubated with indicated heparin concentration in Dulbecco's Modified Eagle Medium (DMEM) for 30 min at room temperature. Cells were incubated with AAV/DMEM/heparin solution for 24 h, followed by flow cytometry.

Structural modeling and heparin docking

AAV capsid variants were modeled with the Rosetta software suite for molecular modeling and design^[26] using the RosettaCM protocol^[27] through RosettaScripts.^[28] The structure of AAV2 (Protein Data Bank ID: 6IH9^[29]) was relaxed^[30] and used as a template for all further studies. For heparin docking studies, GlycanDock^[31] was used. For the full protocol including input XML files, see [Supporting Information S1](#). Figures were created with ChimeraX.^[32]

Molecular dynamics simulations

For system solvation with TIP3P water molecules, the solution builder of CHARMM-GUI^[33] was used, and charge was neutralized with NaCl. All simulations used the Amber ff19sb force field.^[34] Calculations were performed with the Amber molecular dynamics (MD) package using the pmemd software.^[35] After an initial minimization step, Langevin dynamics with a friction coefficient of 1 ps⁻¹ was used for linear heating of the system in constant volume for 1 ns, during which the protein was positionally restrained with a final equilibrium temperature of 303.15 K. An NPT simulation was performed using the Monte Carlo barostat to control the isotropic pressure scaling, where N denotes the constant particle number, P equals pressure and T is the temperature. Electrostatic interactions were calculated using a long-distance cutoff of 9 Å. For each variant, three 500 ns long simulations were performed. For minimization, equilibration, and production run input files, see [Supporting Information](#) (Movies [S1](#), [S2](#), [S3](#)). Trajectories were analyzed with pytraj,^[35] a python package binding of cpptraj,^[36] and visualized with VMD.^[37]

Statistical analysis

All statistical analyses were performed in GraphPad Prism 6 (GraphPad Software).

Data were log₁₀-transformed except for data representing folds and parts of the whole. Multiple group comparisons were analyzed with an ordinary one-way ANOVA or two-way ANOVA, followed by Tukey's post-hoc test. If a control column was available (e.g., "AAV2"), the remaining groups were tested against the control column and corrected with Dunnett's test for multiple comparisons.

Results with a *p* value ≤ 0.05 were considered statistically significant.

(For further methods, see the extended methods.)

RESULTS

MLIV.K and MLIV.A identified as most abundant AAV capsid variants by *in vivo* selection

After *in vivo* high-throughput selection of an AAV2 peptide display library initially designed by Perabo et al.^[18] in two distinct HCC mouse models,^[16,17] we isolated viral genomes from the nuclear fraction of liver (nontumor) tissue, followed by NGS ([Figure 1](#)). The most enriched variants, MLIV.R and MLIV.GA, had to be excluded from further analysis because they were overrepresented in the original unselected libraries (MLIV.GA) or nonspecifically enriched, i.e., independent from the target tissue-specific selection process, during library production (MLIV.R). Thus, MLIV.AQ, MLIV.K, MLIV.G, and MLIV.A, the next most enriched variants, were vectorized ([Figure 1B, C](#)), with MLIV.K and MLIV.A meeting our criteria of titers ≥ 2 × 10¹¹/ml ([Table S1](#)).

Improved murine and human hepatocyte tropism compared with the parental AAV2

We used a conventional replication-competent rep-cap_{mod} library, and thus capsid variants had been selected for accumulation in the target cell nucleus but not for their ability to express a transgene. MLIV.K and MLIV.A were therefore first assayed for transgene expression (functional transduction) in primary hepatocytes ([Figure 2A](#)). For comparison, we included AAV2, the serotype that served as backbone for our library, and AAV8, considered as a state-of-the-art reference for *in vivo* liver transduction.^[38] Both variants efficiently transduced primary human and murine hepatocytes (PHH and PMH). In particular, MLIV.K showed significantly higher transduction efficiencies than AAV2 (PHH: 6-fold; PMH: 5-fold), and both

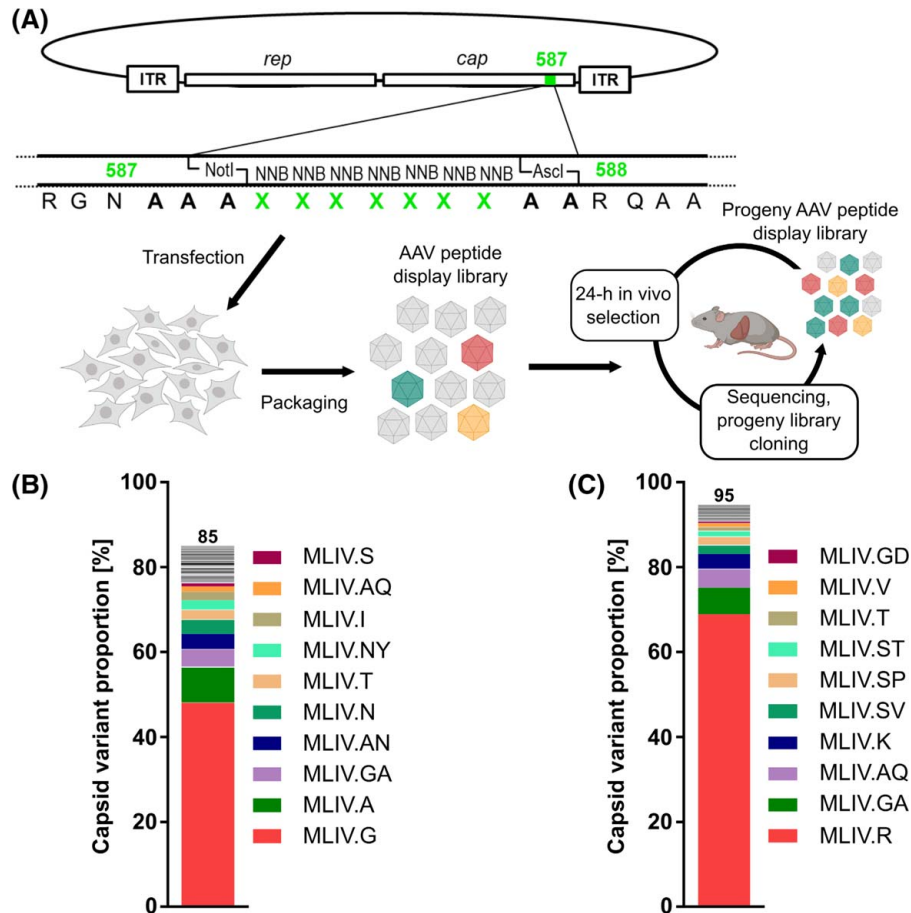


FIGURE 1 Schematic representation of *in vivo* high-throughput adeno-associated virus (AAV) peptide display selection and capsid variant contribution to the total pool. (A) AAV2 peptide display library production and *in vivo* high-throughput selection. The 50 most abundant capsid variants identified in the nontumor liver tissue of (B) transforming growth factor (TGF) α/c -myc hepatocellular carcinoma (HCC) mouse model and (C) Hepa129-grafted HCC mouse model after three rounds of *in vivo* selection. Proportion of variants on total pool is presented as percentage, setting total next-generation sequencing reads in the nontumor liver tissue to 100%. The total percentage of the 50 most abundant capsid variants is indicated. The 10 most abundant capsid variants are listed and color-coded. Cherry red (lowest bar) to dark purple (top bar) equals the first to the tenth rank. Capsid variants with the same nomenclature are identical and were found in both models. ITR, inverted terminal repeat; NNB, N represents any of the four bases, B represents cytosine, guanine, or thymine

capsid variants mediated superior HH transduction compared with AAV8 (MLIV.K/MLIV.A; PHH: 14-/5-fold; PMH: 16-/6-fold).

We subsequently compared MLIV.K and MLIV.A to AAV2 and AAV8 *in vivo*. For MLIV.K and MLIV.A, significantly improved transduction levels were observed in the liver region of healthy BALB/c mice (upper abdomen, Figure 2B, Figure S1). On day 28, animals treated with MLIV variants showed 13- to 26-fold higher Fluc expression levels in the upper abdomen than mice of the AAV2 cohort (Figure 2C). MLIV.A even reached a similar luciferase activity as AAV8. Fluc activity was detectable in liver lysates, whereas transgene expression activity remained at background level in off-target tissue lysates (Figure S2). Vector genome biodistribution analysis confirmed significant detargeting of our capsid variants from spleen, lung, and heart (Figure 2D). The most prominent effect was observed for spleen with 206-fold lower levels for MLIV.K and MLIV.A

compared with AAV2. Furthermore, levels were reduced 25-fold (MLIV.K) and 19-fold (MLIV.A) in lung and 7-fold (MLIV.K and MLIV.A) in heart compared with AAV2. The quantitative polymerase chain reaction analysis also revealed that both variants required significantly fewer vector genomes to outperform AAV2 or equal AAV8 in murine liver transduction, arguing for improved efficacy of MLIV.K and MLIV.A in liver (Figure 2C vs. D).

MLIV.K and MLIV.A provide capsid properties relevant for liver targeting

The two main residues of the AAV2-HSPG binding motif, R585 and R588, are separated at least on the linear sequence when inserting a peptide C-terminal of N587. We therefore analyzed the interaction of MLIV.K and MLIV.A with HSPG. Firstly, we determined the binding affinity (Figure 3A). AAV2 vector particles were

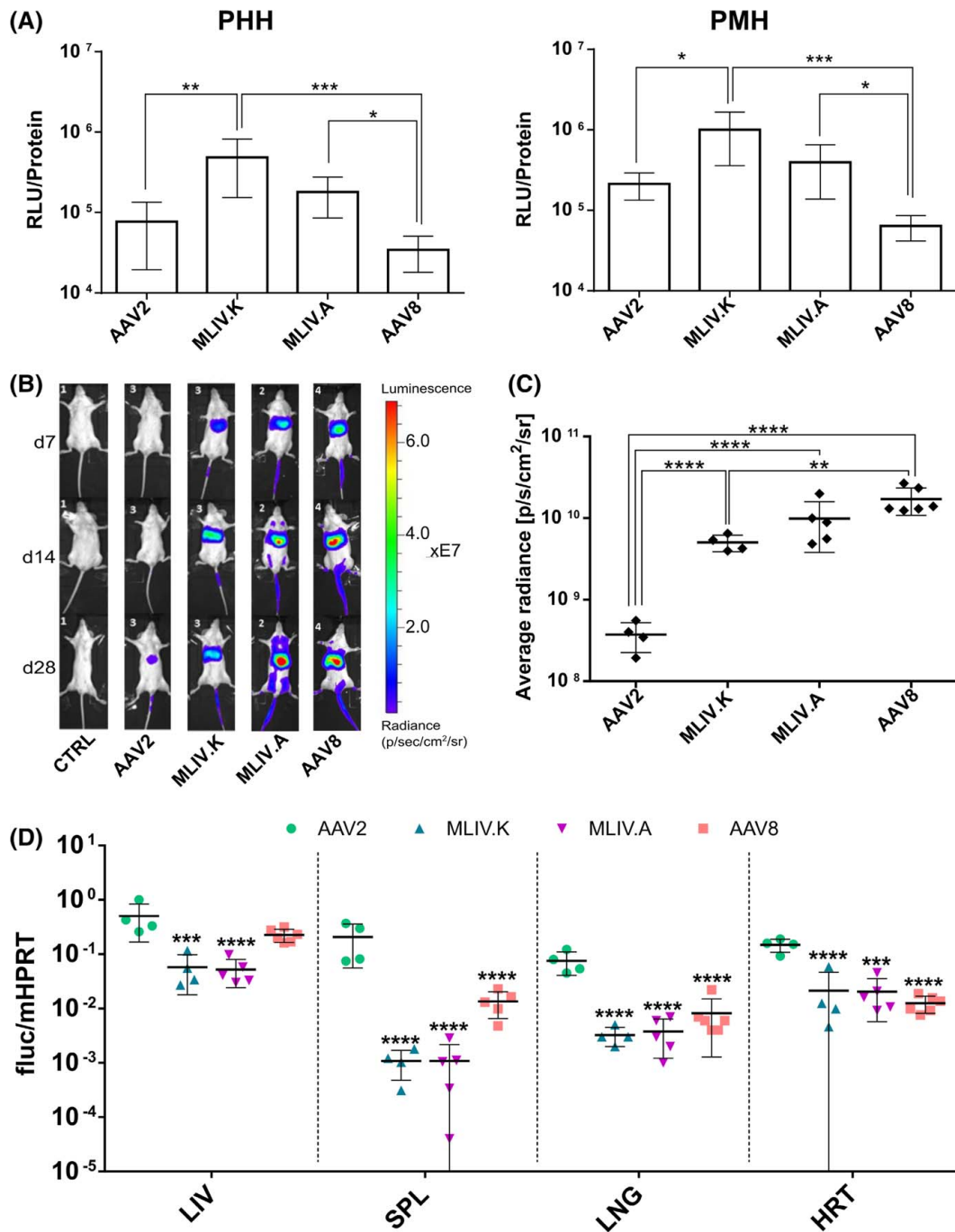


FIGURE 2 MLIV.K and MLIV.A show hepatocyte tropism in primary cells and *in vivo*. (A) Transduction of primary human hepatocytes (PHH; $n = 4$) and primary murine hepatocytes (PMH; $n = 3$) with MLIV.K and MLIV.A compared with adeno-associated virus (AAV) 2 (parental serotype) and AAV8 (state-of-the-art reference). Primary cells were transduced with indicated vectors delivering sc.AAV.SFFV.Fluc (genomic particles of infection [GOI] 1×10^4). After 72 h, firefly luciferase (Fluc) activity was measured as relative light units (RLU) in cell lysates by luciferase assay and normalized to total protein content. Data shown in \log_{10} -scale as mean RLU/protein with SD. (B) Animals were intravenously (i.v.) injected with 5×10^{11} particles of indicated vectors delivering sc.AAV.SFFV.Fluc genomes, and Fluc was monitored for 28 days. Representative images of *in vivo* imaging system (IVIS) measurements at day 7 (d7), day 14 (d14), and day 28 (d28). AAV2: $n = 4$; MLIV.K: $n = 4$; MLIV.A: $n = 5$; AAV8: $n = 6$. CTRL (nontreated): $n = 2$. (C) Average radiance (p/s/cm²/sr) measured over liver on day 28. Data shown in \log_{10} -scale as average RLU with means and SD. (D) AAV vector genomes measured by relative quantitative polymerase chain reaction (qPCR) quantification of DNA samples isolated from liver (LIV), spleen (SPL), lung (LNG), and heart (HRT) on day 28. Data shown in \log_{10} -scale as efficiency-scaled ratio of Fluc to murine hypoxanthine-guanine phosphoribosyltransferase (mHPRT) with means and SD. Statistics: (A,C) ordinary one-way ANOVA with \log_{10} -transformed data. (A: $p = 0.0006$; C: $p < 0.0001$); Tukey's multiple comparisons; (D) two-way ANOVA within each tissue group with \log_{10} -transformed data. (Interaction tissue/AAV: $p \leq 0.001$; tissue: $p \leq 0.0001$; AAV: $p \leq 0.0001$); Dunnett's multiple comparisons with AAV2 as control group; * $p < 0.05$; ** $p < 0.01$; *** $p < 0.001$; **** $p \leq 0.0001$

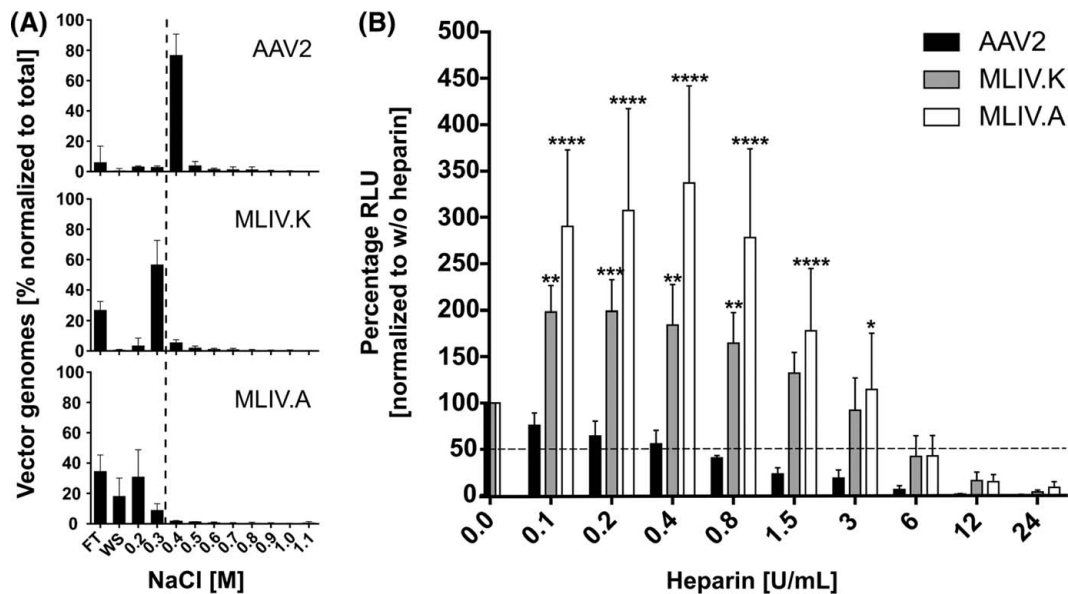


FIGURE 3 Reduced affinity and dependency of MLIV variants on heparan sulfate proteoglycan (HSPG) compared with adeno-associated virus (AAV) 2. (A) Heparin affinity chromatography of MLIV.K and MLIV.A compared with AAV2 ($n = 3$). Vectors encoding for sc.CMV.GFP were loaded on a heparin affinity column, and flow-through (FT) and wash (WS) fraction were collected. AAVs were eluted by a salt gradient of sodium chloride (NaCl) (0.2–1.1 M) in PBS/MgCl₂/KCl (wash buffer [0.137 M NaCl]), and elution fractions were collected. Samples were quantified by quantitative polymerase chain reaction (qPCR). Data are shown in linear scale as mean percentage of total vector genomes with SD. (B) Heparin competition assay with MLIV.K and MLIV.A compared with AAV2 on Pop10 hepatocyte cell line ($n = 4$). Indicated vectors delivering sc.SFFV.Fluc were preincubated with increasing heparin concentrations (0–24 U/ml) for 30 min at RT, thereafter Pop10 were transduced with genomic particles of infection (GOI) 1×10^3 . After 24 h, luciferase activity in cell lysates was measured and normalized to mock-treated AAV (0 U/ml heparin) transduction. Data are shown in linear scale as mean relative light units (RLU) in % of mock-treated with SD. Statistics: two-way ANOVA within each heparin concentration group (Interaction concentration/AAV: $p < 0.0001$; concentration: $p < 0.0001$; AAV: $p < 0.0001$; concentration: $p < 0.0001$; AAV: $p < 0.0001$); Dunnett's multiple comparisons with AAV2 as the control group; * $p < 0.05$; ** $p < 0.01$; *** $p < 0.001$; **** $p < 0.0001$

eluted from a heparin affinity column at 0.4 M NaCl. In contrast, MLIV.K showed reduced binding with 27% of the vector genomes detected in the flow-through. Heparin-bound MLIV.K particles (57%) were eluted at a salt concentration of 0.3 M, indicating a lower affinity. For MLIV.A, 35% and 18% of vector genomes were detected in the flow-through and wash fractions, respectively, and column-bound MLIV.A particles (31%) were already eluted with 0.2 M NaCl.

To confirm the lower affinity, we performed a heparin competition assay. For AAV2, transduction efficiency was reduced by half (IC_{50}) in the presence of ~ 0.4 U/ml of heparin (Figure 3B). The same concentration did neither impair MLIV.K nor MLIV.A and—in contrast—remarkably enhanced transduction efficiency. Increasing the heparin concentration inhibited transduction with an IC_{50} value of ~ 6.0 U/ml (~ 15 -fold higher).

Huttner et al. reported that peptide insertion C-terminal of N587 can confer immune escape properties.^[39] We therefore incubated our capsid variants with serial dilutions of human IVIG and individual human donor serum samples. Again, AAV2 and AAV8 served as references. In comparison, both variants revealed distinct neutralization profiles with a moderate immune escape phenotype (Figure S3).

We previously reported that capsid stability and uncoating efficiency correlates,^[10] with the latter being a key determinant for transduction efficiency. We therefore performed a thermostability assay (Figure S4). Both variants showed comparable stability, which differed from AAV2. Specifically, the A20 signal faded for both variants when reaching temperatures of 60.7°C, not affecting AAV2 capsids (strong A20 and lack of B1 signals, respectively). Simultaneously, B1 signal became detectable for both variants at that temperature, revealing capsid disassembly.

Modeling of altered heparin-binding properties of MLIV.K and MLIV.A

To explain the altered heparin-binding properties of MLIV.K and MLIV.A (Figure 3), we performed a structure-driven analysis of the capsids. Figure 4A depicts an overlay of the tertiary structure of the variable region (VR)VIII loop of AAV2 with MLIV.K and MLIV.A. Both inserted peptides mainly consist of small and flexible amino acids, resulting in a disordered secondary structure with small helical fragments in our models.

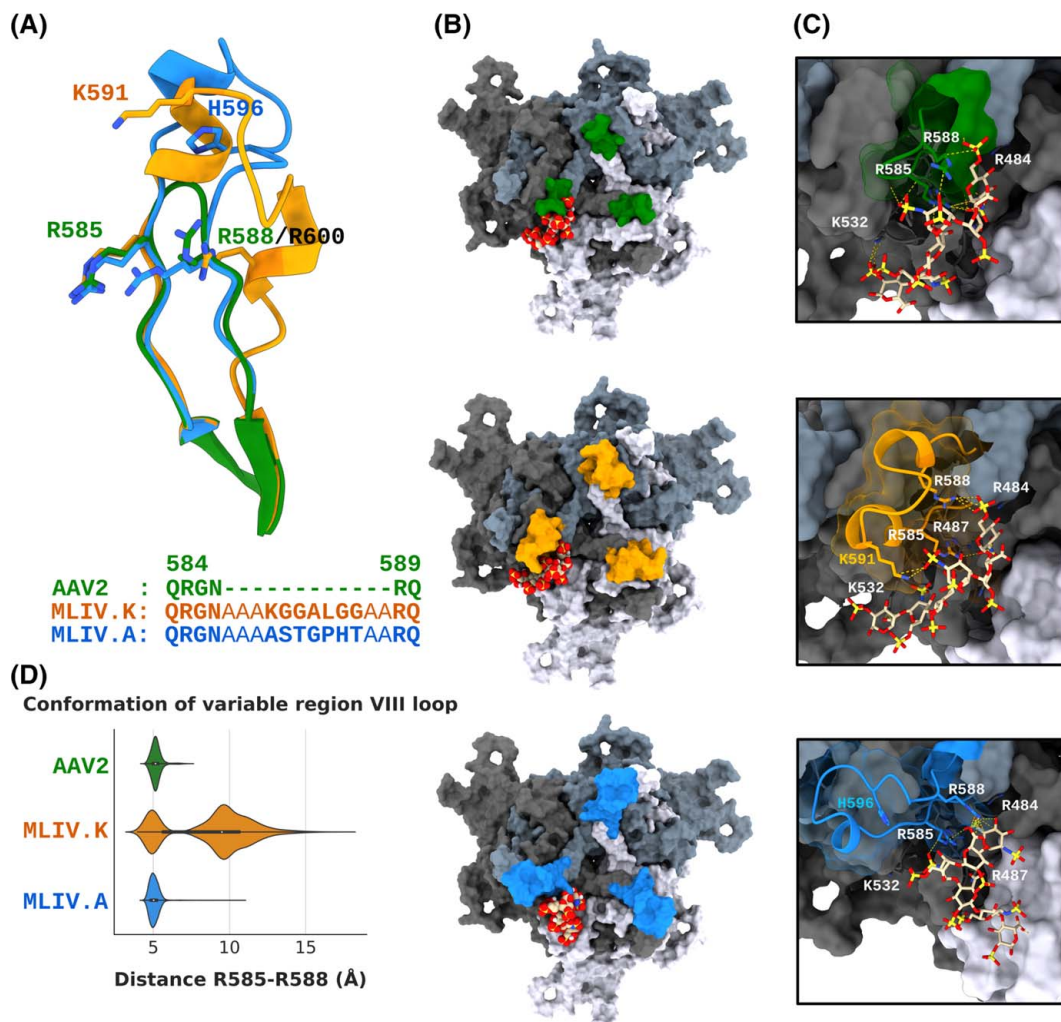


FIGURE 4 Comparison of adeno-associated virus (AAV) 2 structure and heparin binding to structural models of MLIV.K and MLIV.A. (A) Overlay of variable region (VR)VIII loop tertiary structure of MLIV.K (orange) and MLIV.A (blue) with AAV2 (green). Capsid variant sequences include wild-type AAV2 sequence RGN[...]R and left (AAA) and right (AA) peptide linker. Highlighted AA residues are illustrated as stick representation. (B) Surface model of heparin docking in the heparin-binding pocket of AAV2, MLIV.K, and MLIV.A viral protein (VP) 3 trimer. (C) Closeup of heparin interactions with the VR VIII loop, with crucial residues highlighted in stick representation. For clarity, residue numbering follows the AAV2 numbering scheme, with exception of K591 (in peptide insertion of MLIV.K, orange) and H596 (in peptide insertion of MLIV.A, blue). (D) Violin plot of the distance between R585 and R588/R600 in AAV2, MLIV.K, and MLIV.A MD simulations. For each variant, three 500 ns long simulations were performed

Using structural modeling and docking, we subsequently modeled how the capsid variants might interact with heparin using information available for AAV2 as a reference point. In the case of AAV2, heparin contacts R585, R588, R484, and K532, with the HSPG binding motif being constituted by two AAV capsid subunits^[40] (Figure 4B,C). For MLIV.K, the model predicts heparin to bind to R585, R588, R484, and K532 despite the peptide insertion between N587 and R588. In contrast, the predicted structure of the peptide insertion of MLIV.A interferes with heparin binding to K532 but allows R585, R588, and R484 binding, albeit in an orientation that differs from AAV2.

As the sequence of the MLIV.K peptide with four glycine residues foretells a highly flexible loop

(Figure 4A), we studied possible conformations of the variants' viral protein (VP) 3 trimer with MD simulations. We investigated changes in the relative distance of R585 and R588 and their orientation toward each other (Figures 4D and S5). Unsurprisingly, the loop of AAV2 possesses a single conformation with a distance between R585 and R588 normally distributed around 5 Å. Similarly, a single conformation around 5 Å was observed for MLIV.A, with the peptide insertion sterically impairing HSPG to bind to K532, as reflected in our heparin docking experiments (Figure S5). Therefore, a lower heparin-binding affinity for MLIV.A would be likely, as observed experimentally (Figure 3). In contrast, the flexible structure of MLIV.K can adapt alternative conformations distributed around 9 Å. Thereby, the MLIV.K peptide insertion engages at

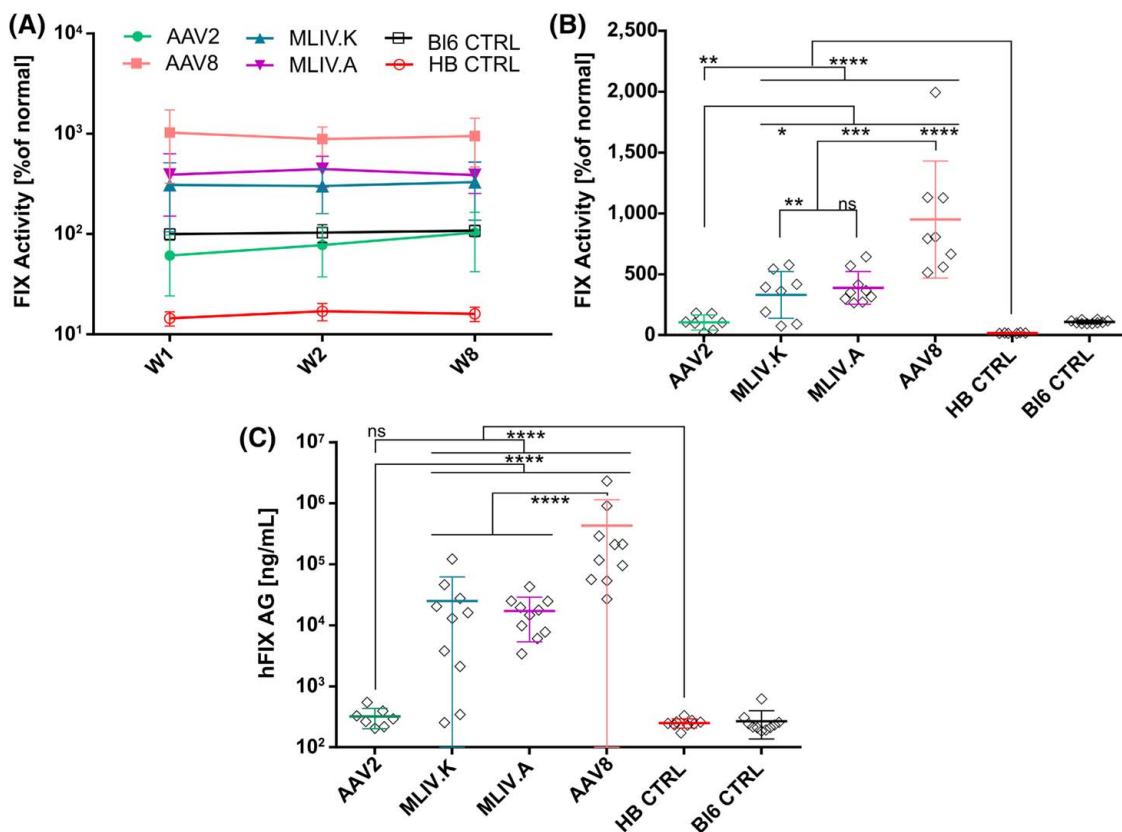


FIGURE 5 Capsid variants mediate correction of blood clotting factor 9 (FIX) deficiency in hemophilia B (HB) mice. Animals were administered with 5×10^{10} particles of indicated vectors delivering scAAV.LP1.hFIX genomes. HB CTRL: nontreated HB (FIX^{-/-}) mouse model; BI6: healthy mouse control. (A) FIX activity analyzed by activated partial thromboplastin time (aPTT) measurement at 1 week (W1), 2 weeks (W2), and (A + B) 8 weeks (W8) post transduction (p.t.), normalized to human serum reference standard; because of background blood clotting effects, all samples were spiked with HB serum. Data shown in (A) log₁₀-scale and (B) linear scale as FIX activity in % of normal FIX activity with mean and SD. (C) Human blood clotting factor (hFIX) serum level analyzed by enzyme-linked immunosorbent assay (ELISA) W2 p.t.; normalized to human serum reference standard. Data shown in log₁₀-scale as hFIX antigen (AG) in nanograms per milliliter with mean and SD. Animal cohorts aPTT: adeno-associated virus (AAV) 2 n(W1) = 6/n(W2) = 7/n(W8) = 7; MLIV.K n(W1) = 9/n(W2) = 10/n(W8) = 8; MLIV.A n(W1) = 8/n(W2) = 10/n(W8) = 9; n(W1) = 8/n(W2) = 10/n(W8) = 9; AAV8 n(W1) = 10/n(W2) = 10/n(W8) = 8; HB CTRL: n(W1) = 9/n(W2) = 9/n(W8) = 6; BI6 CTRL: n(W1) = 9/n(W2) = 10/n(W8) = 10. Animal cohorts ELISA: AAV2 n(W1) = 6/n(W2) = 7/n(W8) = 6; MLIV.K n(W1) = 9/n(W2) = 10/n(W8) = 1 n(W1) = 8/n(W2) = 10/n(W8) = 9; MLIV.A n(W1) = 7/n(W2) = 10/n(W8) = 3; AAV8 n(W1) = 8/n(W2) = 10/n(W8) = 4; HB CTRL: n(W1) = 9/n(W2) = 9/n(W8) = 3; BI6 CTRL: n(W1) = 9/n(W2) = 10/n(W8) = 5. Statistics: (B,C) ordinary one-way ANOVA with log₁₀-transformed data, Tukey's multiple comparisons; **p* < 0.05; ***p* < 0.01; ****p* < 0.001; *****p* < 0.0001. For simplification, the statistical significances of AAV2 vs. MLIV.K and MLIV.A; AAV8 vs. MLIV.K and MLIV.A; and HB CTRL vs. MLIV.K and MLIV.A are shown exclusively (see Supporting Information S6 for complete post-hoc *p*-value reports).

least two transient conformational states of a partially covered and uncovered heparin-binding pocket. Docking heparin to these two conformations highlighted that only one is binding heparin (Figure S6), in line with the experimental data (Figure 3). Rendered movies of the MD trajectories can be found in Movies S1, S2, and S3.

Up to 400% of physiological FIX activity in FIX-knockout mice treated with MLIV variants

To challenge our capsid variants, we i.v. injected FIX^{-/-} HB mice with a dose of 5×10^{10} vg encoding for human FIX, which corresponds to the low-dose

regimens in liver-directed preclinical gene therapy approaches.^[4] All AAV vectors rescued blood clotting in the HB model to the levels observed in healthy BI6 control animals. For AAV2, therapeutic effect ranged around 100% of physiological FIX activity. In contrast, MLIV.K and MLIV.A mediated 300%–400% of physiological FIX activity, respectively. Strikingly, mice that had received MLIV.A reached FIX activity comparable with the AAV8 cohort (Figure 5A,B). Albeit administered at a rather low dose, already 1 week postadministration, all AAV vector-treated animals, except those receiving AAV2, reached their maximum FIX activity. In line with the FIX activity, hFIX serum levels after 2 weeks revealed 54- to 79-fold higher hFIX antigen levels for the MLIV mouse cohorts compared with mice receiving AAV2 (Figure 5C).

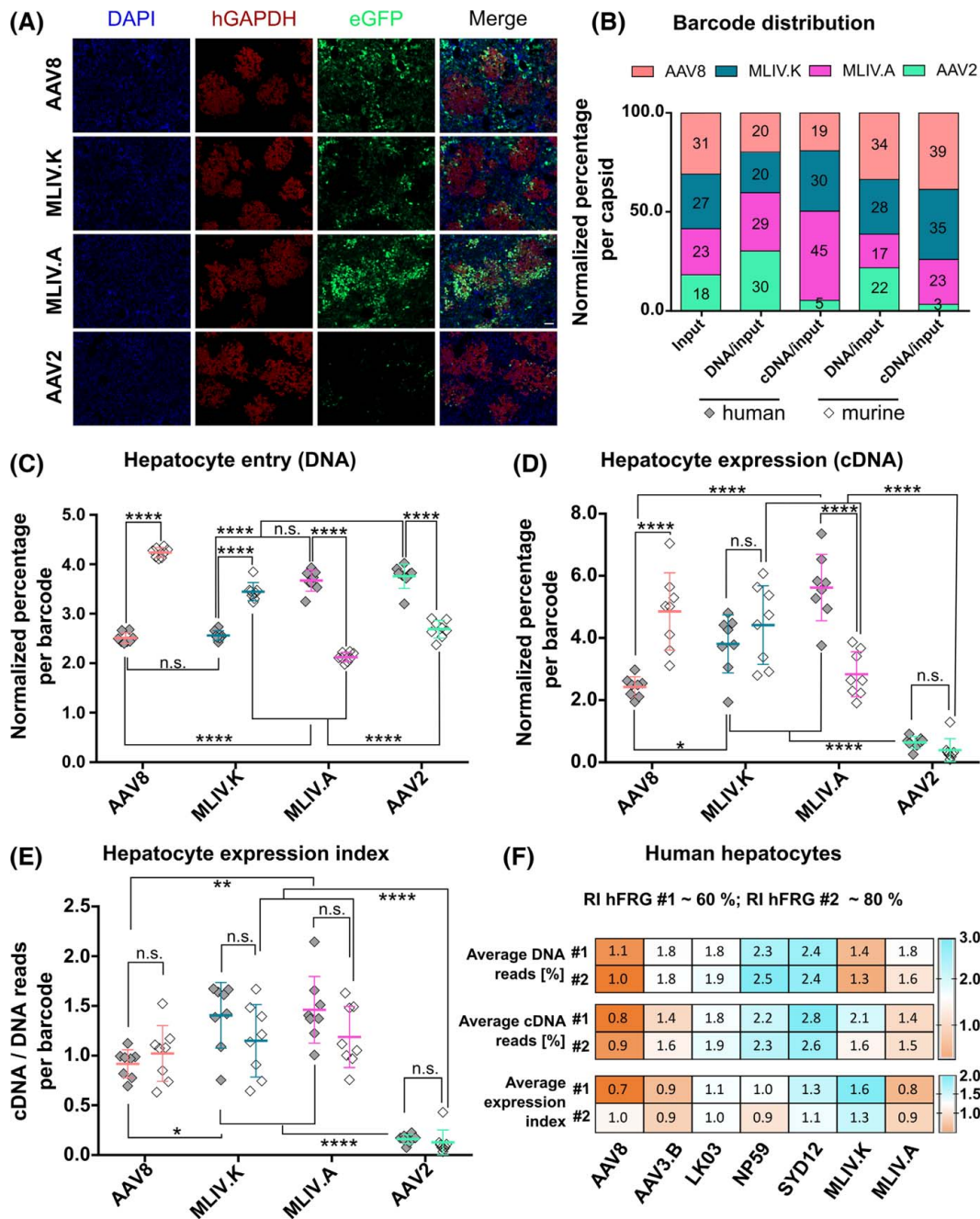


FIGURE 6 MLIV.K and MLIV.A efficiently transduce human and mouse hepatocytes in the humanized (h)FRG mouse model. (A) Representative immunohistochemical liver tissue analysis of the hFRG mouse model ($n = 1$) administered with 5×10^{10} particles of indicated vectors delivering ss.AAV.LSP.eGFP.BC genomes after 7 days. Red: human glyceraldehyde-3-phosphate dehydrogenase (GAPDH); green: adeno-associated virus (AAV) vector-expressed eGFP; blue: 4',6-diamidino-2-phenylindole (DAPI) (nuclei). Scale bar, 100 μ m. (B–F) *In vivo* comparison of cell entry (DNA) and functional transduction (complementary DNA [cDNA]) of MLIV variants in the xenograft liver of the hFRG mouse model (B–E: $n = 1$; F: $n = 2$) administered with an equimolar pool of the indicated vectors (defined as input) delivering ss.AAV.LSP.eGFP.BC genomes ($n = 8$ uniquely barcoded genomes per capsid, 1×10^{10} particles per capsid) after (B–E) 1 and (F) 2 week(s). (B) Percentages of next-generation sequencing reads assigned to each capsid at entry (DNA reads normalized to input DNA reads) and expression (cDNA reads normalized to input DNA reads) level in human and murine hepatocytes. Data are shown in linear scale as % of reads in parts-of-a-whole bars. (C) Hepatocyte entry index per BC (DNA reads normalized to input DNA reads) in human (gray diamonds) and murine (clear diamonds) hepatocytes. (D) Overall expression per BC in hepatocytes (cDNA reads normalized to input DNA reads) in human and murine hepatocyte populations. (E) Hepatocyte expression index per BC (cDNA reads normalized to DNA reads). (F) Average human hepatocyte entry (DNA reads normalized to input DNA reads), overall expression (cDNA reads normalized to input DNA reads), and expression index (cDNA reads normalized to DNA reads). (C–E) Data are shown in linear scale as the respective ratio (C,D) in % (C–E) with mean and SD. Statistics: (B–E) two-way ANOVA (interaction species/AAV: $p < 0.001$; Species: $p < 0.0001$; AAV: $p < 0.0001$), Tukey's multiple comparisons test; (F) Ordinary one-way ANOVA ($p < 0.0001$), Tukey's multiple comparisons test; For a clear overview, only the following statistical (non)significances are depicted: (C–E) AAV2 human and murine hepatocytes vs. the equivalent hepatocyte population of MLIV.K and MLIV.A; AAV8 human hepatocytes vs. MLIV.K and MLIV.A human hepatocytes; human vs. murine hepatocytes within each group. * $p < 0.05$; ** $p < 0.01$; *** $p < 0.001$; **** $p < 0.0001$ (see Supporting Information S6 for complete post-hoc p -value reports of 6C–F). eGFP, enhanced green fluorescent protein; RI, replacement index

MLIV.K and MLIV.A efficiently transduce human hepatocytes in xenograft mice

MLIV.K and MLIV.A efficiently transduced PMH and PHH in cell culture (Figure 2). To investigate this feature *in vivo*, we assayed our capsid variants as barcoded enhanced green fluorescent protein–expressing vectors in humanized FRG (hFRG) mice. In line with the previous *in vivo* results (Figures 2 and 5), immunofluorescent imaging revealed enhanced transduction of the murine hepatocyte (MH) population by the variants compared with AAV2 as well as strongly improved transduction of the human hepatocyte (HH) population, in particular for MLIV.A (Figure 6A).

Next, vector preparations ($n = 8$ barcoded genomes/capsid = input DNA) were pooled to an equimolar mix of each capsid type for a direct comparison. Although delivering comparable barcoded vector DNA levels to the HH (Figure 6B), the highest overall expression (detected as complementary DNA [cDNA] reads) was mediated by our variants (Figure 6B,D). Compared with AAV2, significantly more MLIV cDNA/input DNA BC reads were found in HH (6- to 9-fold) and MH (7- to 11-fold) (Figure 6B,D). In detail, MLIV.K and MLIV.A BCs were found in 30% and 45% of cDNA reads of HH, respectively, and in 35% and 23% of MH cDNA reads, respectively, as compared with AAV8 (19% [HH] and 39% [MH]) and AAV2 (5% [HH] and 3% [MH]). Both capsid variants also showed a superior expression index in human and murine hepatocytes (both 9-fold) compared with AAV2 (Figure 6E). Furthermore, AAV8 was significantly less efficient at transgene expression in the HH compared with the MLIV variants (overall expression: up to 2.3-fold lower; expression index: up to 1.6-fold lower, Figure 6D,E).

Next, we compared our variants with AAV3.B and capsid variants, all known for their preference for HH. The latter are LK03,^[12] NP59,^[13] and SYD12,^[14] derived from high-throughput selection screens of capsid shuffled libraries. As described before, hFRG mice were injected by a BC vector pool including AAV8 as control based on its MH tropism. HH were isolated by FACS and analyzed for DNA and cDNA BC reads by NGS (Figure 6F). Interestingly, although our capsid variants show HH and MH tropism in hFRG mice (Figure 6D,E)—a challenge when compared with variants with a clear preference for HH—they showed solely a 1.5-fold (MLIV.K) and 1.9-fold (MLIV.A) lower average HH transgene expression (cDNA/input DNA) than the most efficient capsid SYD12. In addition, both variants showed comparable transduction efficiency to LK03 and its closest relative, AAV3.B (Figure 6F). These results were substantiated on protein level in PHH, in which AAV3.B was even outperformed by MLIV.K and MLIV.A (2.8- and 2.5-fold respectively, $n = 1$, Figure S7).

DISCUSSION

AAV vectors have proven their potential as *in vivo* gene delivery tools, especially in liver-directed clinical trials. Nevertheless, there is ample room for improvement. Consequently, research focuses on improving vector efficacy to lower doses in clinical applications and on reducing sensitivity toward preexisting anti-AAV neutralizing antibodies. Regarding translatability, next-generation vectors ought to show a comparable tropism across species, a caveat of natural serotypes. Here, we report on MLIV.K and MLIV.A, derived from an AAV2 peptide display library screen in mice, which possess all of these properties.

The MLIV capsid variants clearly differ from AAV2 and AAV8 because they transduce both primary human and murine hepatocytes *in vitro* and *in vivo* with high efficiency (Figures 2 and 6). Regarding the latter, barcoded MLIVs were applied to hFRG mice, revealing not only efficient liver transduction but also superiority to AAV2 or AAV8 in transducing HH *in vivo* (Figure 6). The observation of enhanced ratios of transcript reads (cDNA) to vector genome reads (DNA) in human and murine hepatocytes, indicates that our capsid variants are processed differently in both species (9-fold higher than AAV2, Figure 6E). The improved liver transduction compared with AAV2 is accompanied by detargeting from common off-target tissues contributing to vector safety (Figures 2B–D and S2). Vector efficacy is further highlighted by results from our murine HB mouse model (Figure 5), in which a relatively low dose ($\sim 2.5 \times 10^{12}$ vg/kg body weight [BW]) mediated the rescue of a minimum of 300% of regular FIX activity.

The success of directed evolution approaches is based on the possibility of screening large AAV capsid libraries for variants that efficiently transduce the respective target cells. With the exception of our MLIV variant screen and a single further study, which was reported while preparing the revision of this manuscript,^[41] to the best of our knowledge, only shuffled capsid libraries have been explored by *in vivo* screens for liver-directed gene therapy so far. The first and so far most promising capsid shuffled variant selected for liver-directed gene therapy is LK03.^[12] LK03, which has close homology to AAV3.B, was selected in hFRG mice and transduces HH with remarkable efficiency. More recent examples of shuffled capsid variants that clearly outperform natural AAV serotypes are NP40, NP59,^[13] and SYD12.^[14] Instead of combining natural AAV capsid sequence motifs or domains, AAV peptide display libraries explore the inherent features of a single AAV capsid backbone and genetically inserted random peptide sequences that affect capsid properties. These are exemplified by changes in thermal stability (Figure S4), which correlate with uncoating efficiency,^[10] a rate-limiting step in

transduction,^[9,10] and by changes in the host interaction both at the pre- and post-entry level (Figures S3 and 3).

Our study explores an *in vivo* AAV peptide display library for variants with improved hepatocyte tropism in an adenovirus-free selection approach in immunocompetent mouse models, whereas other studies have either selected *in vitro*^[42] or, most recently, in hFRG mice.^[41] As an alternative strategy to adding peptide insertions with random sequences, Havlik and colleagues permuted capsid loop structures.^[43] This strategy—applied as *in vitro* screen on a hepatocyte cell line—led to the identification of hum.AAV8. Because the latter so far was investigated with a notably higher dose (5×10^{13} vg/kg BW), it is not possible to compare results reported for hum.AAV8 with our MLIV variants. However, for the promising capsid shuffled variants LK03,^[12] NP59,^[13] and SYD12^[14] as well as HH tropic AAV3.B, we performed a direct comparison in hFRG mice (Figure 6F). This comparison revealed that our variants showed a comparable average efficiency to AAV3.B and LK03 but failed to match SYD12, the most efficient variant in mediating HH transduction, by 1.5 to 1.6-fold. These results were surprising as we expected that MLIV.A and MLIV.K would be “decoyed” by the mouse hepatocyte population^[14] because our variants did not seem to prefer HH in the simultaneous presence of human and murine hepatocytes in hFRG mice (Figure 6).

The improved liver transduction efficiencies of MLIV.A and MLIV.K argued for changes in the host–vector interaction, which we investigated regarding their interaction with HSPG, the natural attachment receptor of AAV2 (Figures 3, 4, S5, and S6). Both variants showed significantly reduced heparin/HSPG binding capabilities. MLIV.A and MLIV.K thereby confirmed the previously published results on AAV2-based variants that transduced hepatocytes with higher efficiency with respect to reduced heparin/HSPG binding capability compared with AAV2.^[24,44] Furthermore, the sterically impaired heparin binding of K532 on the MLIV.A capsid resembles the reduced heparin affinity of the K532E mutants in general^[13,45] and correlates with the enhanced hepatotropism of K532E mutant NP40.^[13] This improved host–vector interaction that is due to low-affinity HSPG binding may lead to advantages in accumulation^[46] and entry,^[6] and might facilitates release from the glycan and thereby likely enhances intracellular vector processing.^[47] These features are combined in MLIV.A and MLIV.K with peptide insertions directing our variants toward an entry receptor, as shown for other peptide display selected variants,^[16,48,49] which distinguishes our variants from shuffled or point-mutated variants. Although the receptor identity remains to be elucidated, the receptor interaction enables MLIV.K and MLIV.A to transduce hepatocytes of different species.

Besides high vector doses and off-target transduction, preexisting antibodies in the human population, particularly against AAV2, are acknowledged as a challenge for the AAV vector system. Corresponding to the peptide insertion site (C-terminal of N587), we expect differences in response to sera with anti-AAV2 neutralizing antibodies (NAbs) that recognize epitopes at the threefold symmetry axis of the capsid - the capsid area we modified.^[39,50] Nevertheless, this can be sufficient to enable transduction at a serum concentration, which neutralizes the parental serotype.^[39,50] For MLIV.A and MLIV.K, we observed that the peptide insertion moderately impacted the sensitivity to human sera, which nevertheless may already be sufficient to make a difference for individual patients. In order to improve the immune escape phenotype, the MLIV peptide insertions might be explored in the context of serotypes with lower seroprevalence than AAV2, e.g., AAV5. Alternatively, as NAb epitopes for AAV2 have been identified and mapped,^[51] the capsid of MLIV.A and MLIV.K could also be subjected to further genetic modifications focusing on those epitopes while maintaining the improved hepatotropism.

In summary, we report on two AAV2-based liver-directed capsid peptide insertion variants, which show promise for overcoming cross-species barriers. Moreover, because of favorable hepatotropism and improved transduction efficiencies, these human-serotype-based variants may represent a valuable advance in the field of liver-directed gene therapy.

AUTHOR CONTRIBUTIONS

Conceptualization, Nadja Meumann, Joachim Schwäble, Leszek Lisowski, and Hildegard Büning; methodology, Nadja Meumann, Marti Cabanes-Creus, Moritz Ertelt, Julie Lucifora, Qinggong Yuan, Liang Zhang, Michael Ott, Albrecht Piiper, Maria Gonzalez-Carmona, Erhard Seifried, Clara T. Schoeder, Joachim Schwäble, Leszek Lisowski, and Hildegard Büning; validation, Nadja Meumann, Marti Cabanes-Creus, Joachim Schwäble, Leszek Lisowski, and Hildegard Büning; formal analysis, Nadja Meumann, Steven R. Talbot; investigation, Nadja Meumann, Marti Cabanes-Creus, Moritz Ertelt, Renina Gale Navarro, Julie Lucifora, Qinggong Yuan, Karin Nien-Huber, Ahmed Abdelrahman, Xuan-Khang Vu, Liang Zhang, Ann-Christin Franke, Christian Schmithals, Albrecht Piiper, Annabelle Vogt, Maria Gonzalez-Carmona, Jochen T. Frueh, Evelyn Ullrich, Philip Meuleman, Margarete Odenthal, Michael Ott, and Joachim Schwäble; resources, Albrecht Piiper, Maria Gonzalez-Carmona, Evelyn Ullrich, Philip Meuleman, Margarete Odenthal, Michael Ott, Erhard Seifried, Clara T. Schoeder, Joachim Schwäble, Leszek Lisowski, and Hildegard Büning; writing—original draft preparation, Nadja Meumann, Hildegard Büning; writing—review and editing, all

authors; visualization, Nadja Meumann, Marti Cabanes-Creus, and Moritz Ertelt; supervision, Albrecht Piiper, Maria Gonzalez-Carmona, Evelyn Ullrich, Philip Meuleman, Margarete Odenthal, Michael Ott, Clara T. Schoeder, Joachim Schwäble, Leszek Lisowski, and Hildegard Büning; project administration, Nadja Meumann and Hildegard Büning; funding acquisition, Albrecht Piiper, Joachim Schwäble, Hildegard Büning. All authors have read and agreed to the published version of the manuscript.

ACKNOWLEDGMENT

The authors would like to thank Maud Michelet and Anaëlle Dubois for help with PHH as well as Prof. Michel Rivoire and his staff from the surgery room for providing us with liver resection. Furthermore, we would like to thank Lieven Verhoye for his support with animal experiments. We would like to thank Barbara Kracher for statistical consultancy. [Figure 1A](#) was created with [BioRender.com](#) (accessed on February 6, 2022). We would like to thank Michael Morgan for his valuable support in English language editing. Open Access funding enabled and organized by Projekt DEAL.

CONFLICT OF INTEREST

Leszek Lisowski owns stock in LogicBio Therapeutics. He received grants from Gyroscope Therapeutics and DiNAQOR. Joachim Schwäble advises BioMarin Pharmaceutical. He received grants from uniQure Biopharma. Hildegard Büning, Nadja Meumann, Joachim Schwäble, and Karin Nien-Huber are filed as inventors in a patent on MLIV.K and MLIV.A held by Fraunhofer-Gesellschaft.

DATA AVAILABILITY STATEMENT

The data presented in this study are available on request from the corresponding author.

ORCID

Nadja Meumann  <https://orcid.org/0000-0003-4929-249X>

Julie Lucifora  <https://orcid.org/0000-0003-0482-7809>

Margarete Odenthal  <https://orcid.org/0000-0002-2424-0960>

Hildegard Büning  <https://orcid.org/0000-0002-3365-6933>

REFERENCES

- ASGCT. Gene, Cell, and RNA Therapy Landscape [Internet]. Q2 2021 Quarterly Data Report. <https://asgct.org/global/documents/asgct-pharma-intelligence-quarterly-report-q1-2021.aspx> (2021). Accessed 6 Feb 2022.
- Keeler AM, Flotte TR. Recombinant adeno-associated virus gene therapy in light of luxturna (and Zolgensma and Glybera): where are we, and how did we get here? *Annu Rev Virol.* 2019;6:601–21.
- Croteau SE, Wang M, Wheeler AP. 2021 clinical trials update: innovations in hemophilia therapy. *Am J Hematol.* 2021;96:128–44.
- Rodríguez-Márquez E, Meumann N, Büning H. Adeno-associated virus (AAV) capsid engineering in liver-directed gene therapy. *Expert Opin Biol Ther.* 2021;21:749–66.
- Boutin S, Monteilhet V, Veron P, Leborgne C, Benveniste O, Montus MF, et al. Prevalence of serum IgG and neutralizing factors against adeno-associated virus (AAV) types 1, 2, 5, 6, 8, and 9 in the healthy population: implications for gene therapy using AAV vectors. *Hum Gene Ther.* 2010;21:704–12.
- Levy HC, Bowman VD, Govindasamy L, McKenna R, Nash K, Warrington K, et al. Heparin binding induces conformational changes in adeno-associated virus serotype 2. *J Struct Biol.* 2009;165:146–56.
- Pillay S, Meyer NL, Puschnik AS, Davulcu O, Diep J, Ishikawa Y, et al. An essential receptor for adeno-associated virus infection. *Nature.* 2016;530:108–2.
- Dudek AM, Zabaleta N, Zinn E, Pillay S, Zengel J, Porter C, et al. GPR108 is a highly conserved AAV entry factor. *Mol Ther.* 2020;28:367–81.
- Thomas CE, Storm TA, Huang Z, Kay MA. Rapid uncoating of vector genomes is the key to efficient liver transduction with pseudotyped adeno-associated virus vectors. *J Virol.* 2004;78:3110–22.
- Rossi A, Dupaty L, Aillot L, Zhang L, Gallien C, Hallek M, et al. Vector uncoating limits adeno-associated viral vector-mediated transduction of human dendritic cells and vector immunogenicity. *Sci Rep.* 2019;9:3631.
- Wang J, Xie J, Lu H, Chen L, Hauck B, Samulski RJ, et al. Existence of transient functional double-stranded DNA intermediates during recombinant AAV transduction. *Proc Natl Acad Sci.* 2007;104:13104–9.
- Lisowski L, Dane AP, Chu K, Zhang Y, Cunningham SC, Wilson EM, et al. Selection and evaluation of clinically relevant AAV variants in a xenograft liver model. *Nature.* 2014;506:382–6.
- Paulk NK, Pekrun K, Zhu E, Nygaard S, Li B, Xu J, et al. Bioengineered AAV capsids with combined high human liver transduction in vivo and unique humoral seroreactivity. *Mol Ther.* 2018;26:289–303.
- Cabanes-Creus M, Navarro RG, Zhu E, Baltazar G, Liao SHY, Drouyer M, et al. Novel human liver-tropic AAV variants define transferable domains that markedly enhance the human tropism of AAV7 and AAV8. *Mol Ther - Methods Clin Dev.* 2022;24:88–101.
- High KA, George LA, Eyster ME, Sullivan SK, Ragni MV, Croteau SE, et al. A phase 1/2 trial of investigational Spk-8011 in hemophilia a demonstrates durable expression and prevention of bleeds. *Blood.* 2018;132:487.
- Schmitz V, Tirado-Ledo L, Tiemann K, Raskopf E, Heinicke T, Ziske C, et al. Establishment of an orthotopic tumour model for hepatocellular carcinoma and non-invasive in vivo tumour imaging by high resolution ultrasound in mice. *J Hepatol.* 2004;40:787–91.
- Hauptenthal J, Bihrer V, Korkusuz H, Kollmar O, Schmithals C, Kriener S, et al. Reduced efficacy of the PI3K inhibitor BI 2536 on the progression of hepatocellular carcinoma due to low intratumoral drug levels. *Neoplasia.* 2012;14:410–9.
- Perabo L, Büning H, Kofler DM, Ried MU, Girod A, Wendtner CM, et al. In vitro selection of viral vectors with modified tropism: the adeno-associated virus display. *Mol Ther.* 2003;8:151–7.
- Zhang L, Rossi A, Lange L, Meumann N, Koitzsch U, Christie K, et al. Capsid engineering overcomes barriers toward adeno-associated virus vector-mediated transduction of endothelial cells. *Hum Gene Ther.* 2019;30:1284–96.
- LeCluyse EL, Alexandre E. Isolation and culture of primary hepatocytes from resected human liver tissue. *Methods Mol Biol.* 2010;640:57–82.

21. Yuan Q, Loya K, Rani B, Möbus S, Balakrishnan A, Lamle J, et al. MicroRNA-221 overexpression accelerates hepatocyte proliferation during liver regeneration. *Hepatology*. 2013;57:299–310.
22. Schuettrumpf J, Herzog RW, Schlachterman A, Kaufhold A, Stafford DW, Arruda VR. Factor IX variants improve gene therapy efficacy for hemophilia B. *Blood*. 2005;105:2316–23.
23. Milanov P, Ivanciu L, Abriss D, Quade-Lyssy P, Miesbach W, Alesci S, et al. Engineered factor IX variants bypass FVIII and correct hemophilia A phenotype in mice. *Blood*. 2012;119:602–11.
24. Cabanes-Creus M, Westhaus A, Navarro RG, Baltazar G, Zhu E, Amaya AK, et al. Attenuation of heparan sulfate proteoglycan binding enhances in vivo transduction of human primary hepatocytes with AAV2. *Mol Ther Methods Clin Dev*. 2020;17:1139–54.
25. Pavlou M, Schön C, Occelli LM, Rossi A, Meumann N, Boyd RF, et al. Novel AAV capsids for intravitreal gene therapy of photoreceptor disorders. *EMBO Mol Med*. 2021;13:e13392.
26. Leaver-Fay A, Tyka M, Lewis SM, Lange OF, Thompson J, Jacak R, et al. ROSETTA3: an object-oriented software suite for the simulation and design of macromolecules. In: *Methods Enzymol*. Volume 487. London: Elsevier; 2011. p. 545–74.
27. Song Y, DiMaio F, Wang RYR, Kim D, Miles C, Brunette T, et al. High-resolution comparative modeling with RosettaCM. *Structure*. 2013;21:1735–42.
28. Fleishman SJ, Leaver-Fay A, Corn JE, Strauch EM, Khare SD, Koga N, et al. RosettaScripts: a scripting language interface to the Rosetta macromolecular modeling suite. *PLoS One*. 2011;6:e20161.
29. Zhang R, Cao L, Cui M, Sun Z, Hu M, Zhang R, et al. Adeno-associated virus 2 bound to its cellular receptor AAVR. *Nat Microbiol*. 2019;4:675–82.
30. Tyka MD, Keedy DA, André I, DiMaio F, Song Y, Richardson DC, et al. Alternate states of proteins revealed by detailed energy landscape mapping. *J Mol Biol*. 2011;405:607–18.
31. Nance ML, Labonte JW, Adolf-Bryfogle J, Gray JJ. Development and Evaluation of GlycanDock: a protein–glycoligand docking refinement algorithm in Rosetta. *J Phys Chem B*. 2021;125:6807–20.
32. Pettersen EF, Goddard TD, Huang CC, Meng EC, Couch GS, Croll TI, et al. UCSF ChimeraX: structure visualization for researchers, educators, and developers. *Protein Sci*. 2021;30:70–82.
33. Singal AK, Kodali S, Vucovich LA, Darley-Usmar V, Schiano TD. Diagnosis and treatment of alcoholic hepatitis: a systematic review. *Alcohol Clin Exp Res*. 2016;40:1390–402.
34. Tian C, Kasavajhala K, Belfon KAA, Raguette L, Huang H, Miguez AN, et al. ff19SB: amino-acid-specific protein backbone parameters trained against quantum mechanics energy surfaces in solution. *J Chem Theory Comput*. 2020;16:528–252.
35. Case DA, Aktulga HM, Belfon KAA, Ben-Shalom IY, Brozell SR, Cerutti DS, et al. Amber 2021. San Francisco: University of California, San Francisco; 2021.
36. Roe DR, Cheatham TE. PTRAJ and CPPTRAJ: software for processing and analysis of molecular dynamics trajectory data. *J Chem Theory Comput*. 2013;9:3084–95.
37. Humphrey W, Dalke A, Schulten K. VMD: visual molecular dynamics. *J Mol Graph*. 1996;14:33–8.
38. Au HKE, Isalan M, Mielcarek M. Gene therapy advances: a meta-analysis of AAV usage in clinical settings. *Front Med*. 2022;8:809118.
39. Huttner NA, Girod A, Perabo L, Edbauer D, Kleinschmidt JA, Büning H, et al. Genetic modifications of the adeno-associated virus type 2 capsid reduce the affinity and the neutralizing effects of human serum antibodies. *Gene Ther*. 2003;10:2139–47.
40. Opie SR, Warrington KH, Agbandje-McKenna M, Zolotukhin S, Muzyczka N. Identification of amino acid residues in the capsid proteins of adeno-associated virus type 2 that contribute to heparan sulfate proteoglycan binding. *J Virol*. 2003;77:6995–7006.
41. Westhaus A, Cabanes-Creus M, Jonker T, Sallard E, Navarro RG, Zhu E, et al. AAV-p40 bioengineering platform for variant selection based on transgene expression. *Hum Gene Ther*. 2022;33:664–82.
42. Raupp C, Naumer M, Muller OJ, Gurda BL, Agbandje-McKenna M, Kleinschmidt JA. The threefold protrusions of adeno-associated virus type 8 are involved in cell surface targeting as well as postattachment processing. *J Virol*. 2012;86:9396–408.
43. Havlik LP, Simon KE, Smith JK, Klinc KA, Tse LV, Oh DK, et al. Coevolution of adeno-associated virus capsid antigenicity and tropism through a structure-guided approach. *J Virol*. 2020;94:e00976-20.
44. Cabanes-Creus M, Hallwirth CV, Westhaus A, Ng BH, Liao SHY, Zhu E, et al. Restoring the natural tropism of AAV2 vectors for human liver. *Sci Transl Med*. 2020;12:eaba3312.
45. Kern A, Schmidt K, Leder C, Müller OJ, Wobus CE, Von Der Lieth CW, et al. Identification of a heparin-binding motif on adeno-associated virus type 2 capsids. *J Virol*. 2003;77:11072–81.
46. Summerford C, Samulski RJ. Membrane-associated heparan sulfate proteoglycan is a receptor for adeno-associated virus type 2 virions. *J Virol*. 1998;72:1438–45.
47. Uhrig S, Coutelle O, Wiehe T, Perabo L, Hallek M, Büning H. Successful target cell transduction of capsid-engineered rAAV vectors requires clathrin-dependent endocytosis. *Gene Ther*. 2012;19:210–8.
48. Sallach J, Di Pasquale G, Larcher F, Niehoff N, Rübsam M, Huber A, et al. Tropism-modified AAV vectors overcome barriers to successful cutaneous therapy. *Mol Ther*. 2014;22:929–39.
49. Tabebordbar M, Lagerborg KA, Stanton A, King EM, Ye S, Tellez L, et al. Directed evolution of a family of AAV capsid variants enabling potent muscle-directed gene delivery across species. *Cell*. 2021;184:4919–38.e22.
50. Gehrke M, Diedrichs-Möhring M, Bogedein J, Büning H, Michalakakis S, Wildner G. Immunogenicity of novel AAV capsids for retinal gene therapy. *Cell*. 2022;11:1881.
51. Bennett A, Keravala A, Makal V, Kurian J, Belbellaa B, Aeran R, et al. Structure comparison of the chimeric AAV2.7m8 vector with parental AAV2. *J Struct Biol*. 2020;209:107433.

How to cite this article: Meumann N Cabanes-Creus M Ertelt M Navarro RG Lucifora J Yuan Q, et al. Adeno-associated virus serotype 2 capsid variants for improved liver-directed gene therapy. *Hepatology*. 2023;77:802–815. <https://doi.org/10.1002/hep.32733>